

Supplementary Information

Title: Cell lysis via acoustically oscillating sharp edges

Authors: Zeyu Wang, Po-Hsun Huang,* Chuyi Chen, Hunter Bachman, Shuaiguo Zhao, Shujie Yang, and Tony J. Huang*

Department of Mechanical Engineering and Materials Science, Duke University, Durham, NC 27708, USA.

E-mail: phuang73@gmail.com and tony.huang@duke.edu

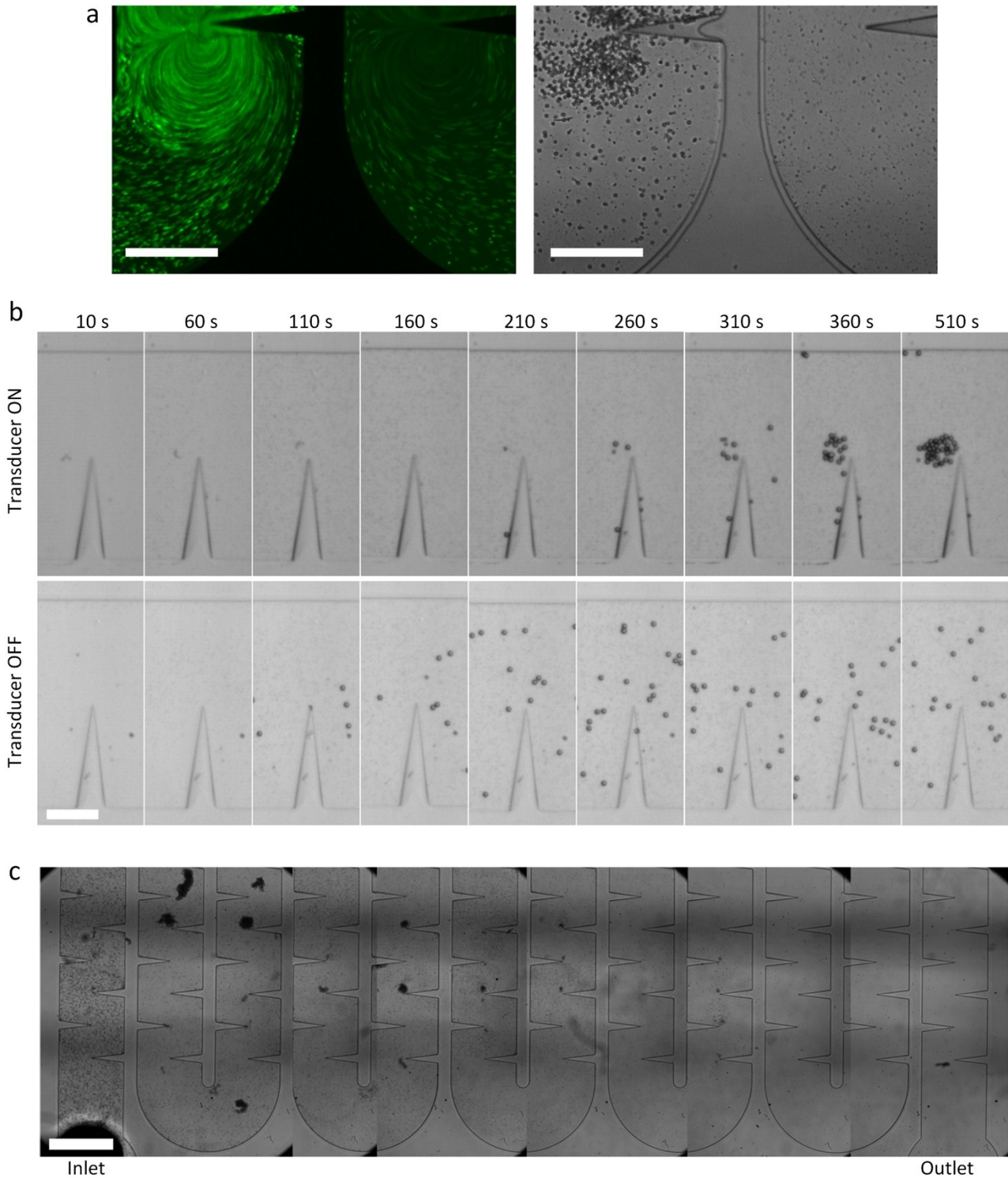


Fig S1. a) Fluorescent and bright-field images showing the number of cells inlet-side and outlet-side in the channel of the acoustofluidic device. b) Acoustic microstreaming vortices' trapping effect on large and small polystyrene beads. All sharp-edge structures in the image are the same sharp-edge. 20 μm and 2 μm beads are mixed and injected into the channel from 0 s. At 10 s, neither 20 μm and 2 μm beads flow to the sharp-edge for both transducer ON and OFF conditions. At 60 s, 2 μm beads flow to the sharp-edge for both transducer ON and OFF condition. When the transducer ON, 20 μm beads flow to the sharp-edge area much slower when the transducer OFF and are trapped around the sharp edge, indicating larger particles effectively trapped by sharp-edge-induced acoustic microstreaming and flow slower in the channel. c) Spliced image of Jurkat cell lysis in the channel after 15 minutes of continuous activation of the system; the cell number decreases from the inlet to the outlet. Scale bar: a) 500 μm , b) 250 μm , c) 1000 μm .

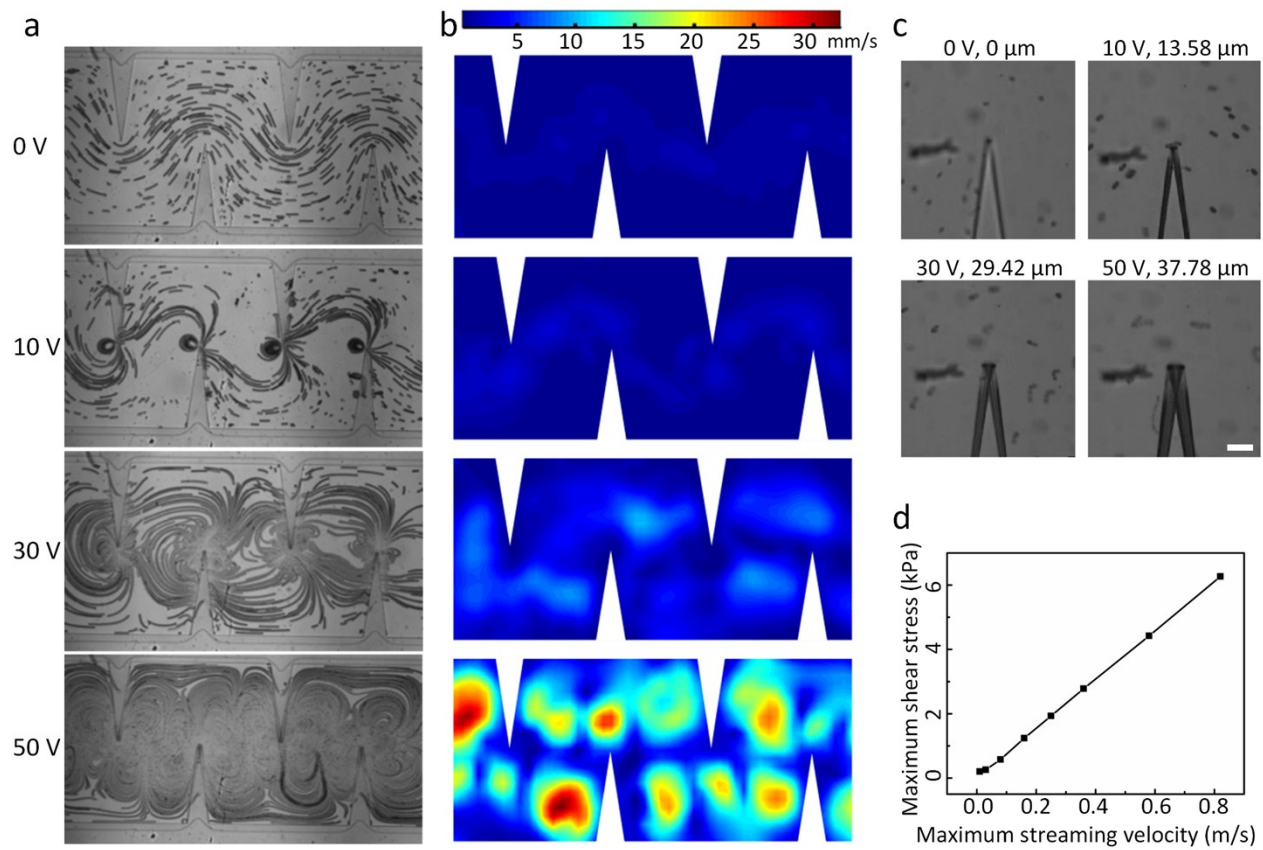


Fig S2. a) Microstreaming pattern demonstrated by the motion of 5 μm polystyrene beads over 0.0667 s; the videos were captured at 3000 fps and images were created by stacking 200 frames. b) Acoustic microstreaming velocity field measured from the fast camera videos and analyzed using PIV software. c) Vibration amplitudes of sharp-edge tips under different transducer excitation voltages. d) Relationship between streaming velocity and shear stress.

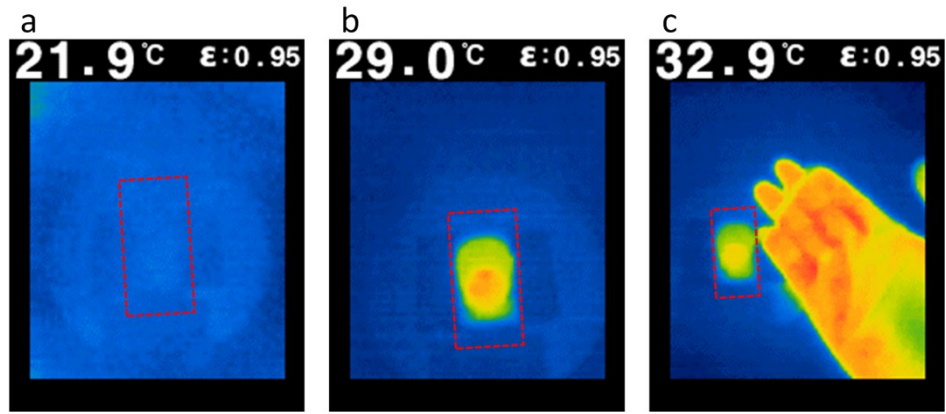


Fig S3. Temperature monitoring over a time interval of 20 minutes: a) temperature before the acoustofluidic device is activated, b) temperature after the acoustofluidic device is activated continuously for 20 minutes, c) temperature comparison between the acoustofluidic device and a human hand (body surface temperature). The red-dashed rectangles mark the perimeter of the device.

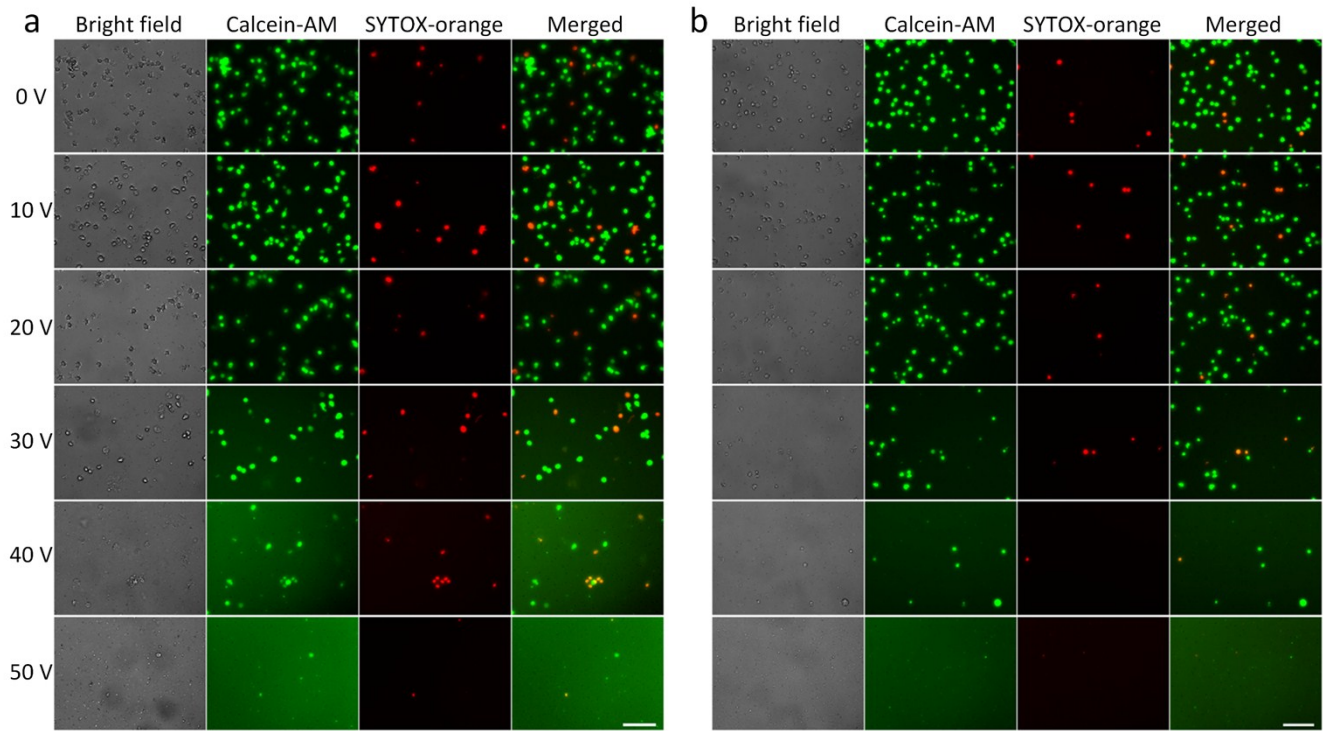


Fig S4. Complete set of images showing the lysis results: a) HeLa cells and b) Jurkat cells under six different driving voltages of the transducer, at a constant flow rate of 5 $\mu\text{L}/\text{min}$. Scale bars: 100 μm .

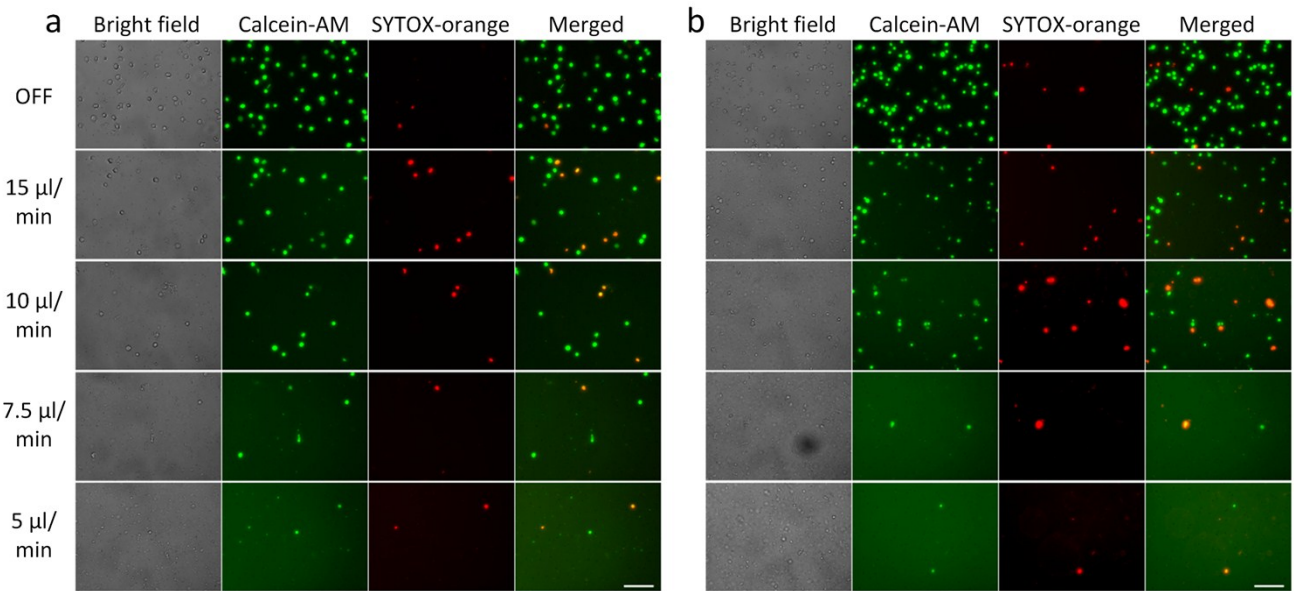


Fig S5. Complete set of images showing the lysis results for a) HeLa cells and b) Jurkat cells at four different sample flow rates, under the same driving voltage of 50 V_{pp}. The images presented in the first row present the results obtained at the flow rate of 15 μL/min but in the absence of acoustic activation. Scale bars: 100 μm.

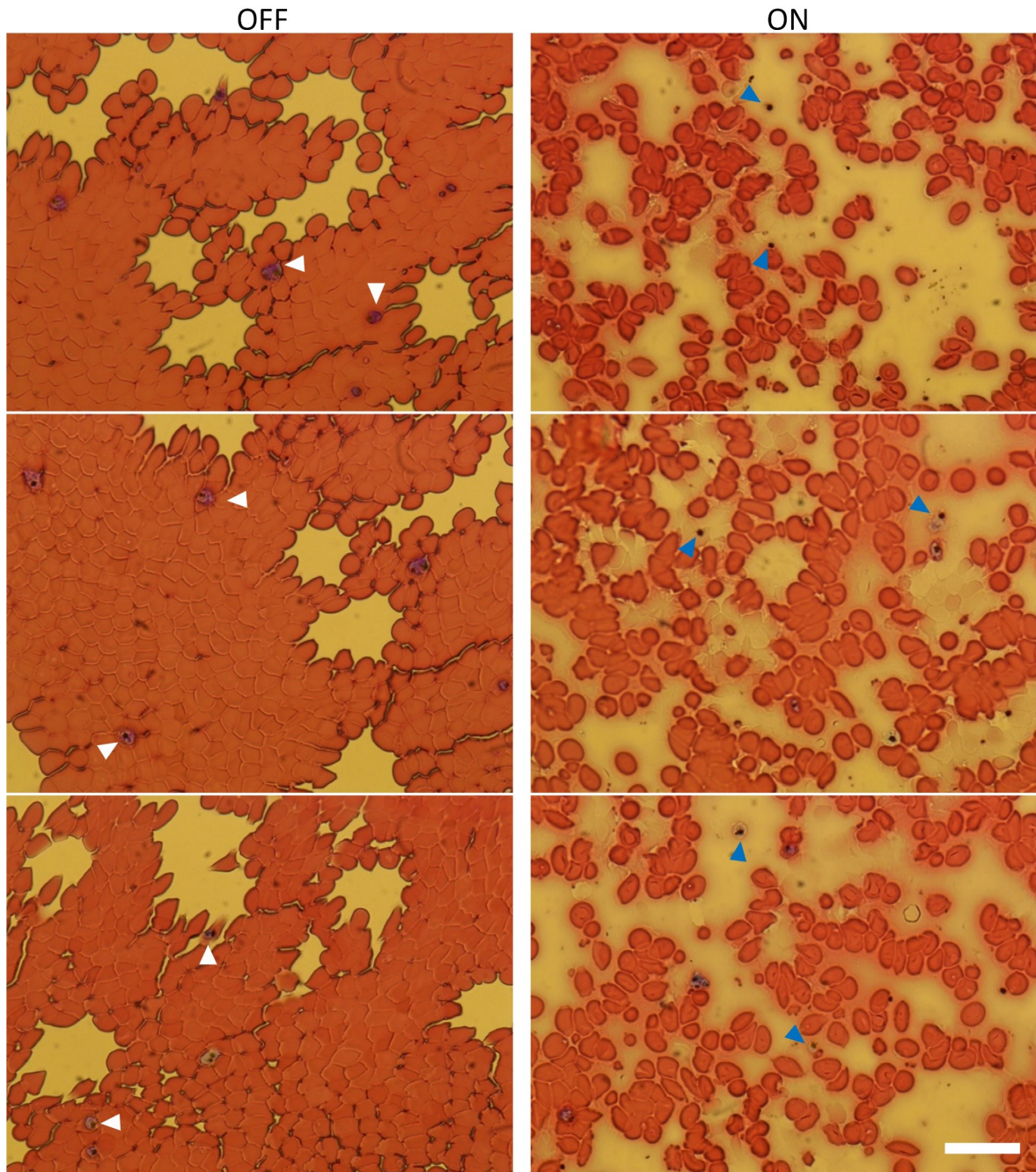


Fig S6. Optical images of malaria-infected RBC lysis samples. The left and right panels present, respectively, the un-lysed samples in the absence of acoustic streaming (OFF) and the lysed samples in the presence of acoustic streaming (ON). The white arrows indicate malaria parasites enclosed by normal RBCs, while the blue arrows indicate parasites released from RBCs (or lysed parasites) because of lysis. Scale bar: 25 μm .

Video captions:

Video S1. Jurkat cell lysis in-channel captured after the system continuously activated for 15 minutes.

Video S2. Trapping effect generated by the acoustic streaming in the channel. The cells are repeatedly flowing through the tips of two nearby sharp-edges and form a bigger particle. This effect provides higher chance of lysis since the cells have higher times of flowing through high shear stress areas during rotating between sharp-edges in the channel.

Video S3. Acoustic streaming patterns shown by fluorescent cells. The flow pattern is consistent with the results in Fig. 2.